



1 **Abstract.** Mineral dust is a major light-absorbing aerosol, which can significantly
2 reduce snow albedo and accelerate snow/glacier melting via wet and dry deposition on
3 snow. In this study, three scenarios of internal mixing of dust in ice grains were
4 analyzed theoretically by combining asymptotic radiative transfer theory and
5 (core/shell) Mie theory to evaluate the effects on absorption coefficient and snow
6 albedo. In general, snow albedo was substantially reduced at wavelengths of $<1.0 \mu\text{m}$
7 by internal dust–snow mixing, with stronger reductions at higher dust concentrations
8 and larger snow grain sizes. Moreover, calculations showed that a non-uniform
9 distribution of dust in snow grains can lead to significant differences in the values of
10 the absorption coefficient and snowpack albedo at visible wavelengths relative to a
11 uniform dust distribution in snow grains. Finally, using comprehensive in situ
12 measurements across the Northern Hemisphere, we found that broadband snow albedo
13 was further reduced by 5.2% and 9.1% due to the effects of internal dust–snow mixing
14 on the Tibetan Plateau and North American mountains. This was higher than the
15 reduction in snow albedo caused by black carbon in snow over most North American
16 and Arctic regions. Our results suggest that significant dust–snow internal mixing is
17 important for the melting and retreat of Tibetan glaciers and North American mountain
18 snowpack.
19



1 1. Introduction

2 Snow cover is one of the most reflective surfaces in the Earth system, and plays a crucial
3 role in the atmospheric solar radiation energy budget via snow albedo feedbacks (Di
4 Mauro et al., 2020; Flanner et al., 2011; Jacobson, 2004; Usha et al., 2020; Xie et al.,
5 2018). Previous studies have shown that light-absorbing particles (LAPs) effectively
6 reduce snow albedo and enhance the absorption of solar radiation after deposition, these
7 studies were based on in situ observations and model simulations (Casey et al., 2017;
8 Hadley and Kirchstetter, 2012; Shi et al., 2020; Warren and Wiscombe, 1980; Yasunari
9 et al., 2012; Yasunari et al., 2015). As a result, snow contaminated with LAPs shows
10 significant changes in morphology (Niwano et al., 2012; Rango et al., 1996), chemistry
11 (France et al., 2012; Reay et al., 2012), hydrology (Matt et al., 2018; Qian et al., 2015;
12 Rahimi et al., 2019), snowmelt rate (Kaspari et al., 2015; Warren, 1984;), and radiative
13 properties (Grenfell et al., 2002; Hansen and Nazarenko, 2004; Zhao et al., 2014).
14 Numerous studies have assessed the potential effects of LAPs, such as black carbon
15 (BC) and mineral dust, on snow albedo by assuming that LAPs mixed outside spherical
16 snow grains (i.e., external mixing) (Flanner et al., 2007; Kokhanovsky, 2013; Libois et
17 al., 2013; Wang et al., 2017; Warren and Wiscombe, 1980). For example, Warren and
18 Wiscombe (1980) calculated snow spectral albedo by solving a radiative transfer
19 equation using Mie theory and δ -Eddington approximations, and found that 10–100 ng
20 g^{-1} of BC and 1–10 $\mu\text{g g}^{-1}$ of dust in old snow decreased albedo by 1%–7% and 2%–
21 10% at 400 nm wavelength, respectively. Flanner et al. (2007) pointed out that the
22 reduction in snow albedo for 1000 ng g^{-1} BC in snow was 0.045 (0.17) with a 50 (1000)
23 μm snow grain radius (R_{ef}) based on the Snow, Ice, and Aerosol Radiation (SNICAR)
24 radiative transfer model. This model utilizes theory from Wiscombe and Warren (1980)
25 and the two-stream radiative transfer solution from Toon et al. (1989). Wang et al. (2017)
26 developed a Spectral Albedo Model for Dirty Snow (SAMDS) based on asymptotic
27 radiative transfer theory, which is a function of the snow grain radius, LAP (e.g., BC,
28 dust) mixing ratios, and the mass absorption coefficients (MACs) of LAPs. Their results



1 revealed that broadband snow albedo decreased 0.03 and 0.003 due to 200 ng g⁻¹ of BC
2 and 2 μg g⁻¹ of dust in snow, respectively, with a R_{ef} of 200 μm.
3 Recently, direct snowpack observations have shown evidence for the existence of LAP–
4 snow internal mixing (e.g., Horhold et al., 2012; Spaulding et al., 2011). LAPs tend to
5 mix externally with snow grains through dry deposition and/or below cloud scavenging,
6 while internal LAP–snow mixing can be produced by nucleation, accretion, riming,
7 aggregation, and sintering during aerosol–cloud–precipitation processes (i.e., wet
8 deposition; Figure 1) (Flanner et al., 2012). Furthermore, Flanner et al. (2012) found
9 that internal BC/ice mixing (IBM) increased the absorption of snowpack by a factor
10 1.8–2.1 relative to external BC/ice mixing (EBM). He et al. (2018) indicated that IBM
11 enhanced the mean snow albedo reduction over the plateau by 30%–60% relative to
12 EBM, based on the updated SNICAR model. Additionally, Dombrovsky and
13 Kokhanovsky (2020) demonstrated that non-uniform BC distribution in ice grains may
14 lead to significantly different absorption coefficients and snowpack albedo in visible
15 (VIS) wavelengths.
16 Numerous studies have addressed the role of IBM in enhancing the absorption of
17 snowpack due to its strong absorption effect relative to other LAPs (Dombrovsky and
18 Kokhanovsky, 2020; Flanner et al., 2012; He et al., 2018; Liou et al., 2011). In contrast,
19 few studies have considered the effects of internal dust/ice mixing (IDM) in snowpack.
20 Dust particles are generally larger than BC, and act as more efficient ice nuclei, showing
21 a better ability to influence cloud formation and precipitation (Creamean et al., 2013;
22 Huang et al., 2014). Therefore, they are more likely to mix internally with ice grains.
23 Furthermore, dust can also dominate light absorption and effectively decrease snow
24 albedo because of its relatively high mass abundance (ppm) in snowpack, especially in
25 areas with seasonal and patchy snow cover or mountainous regions (Di Mauro et al.,
26 2015; Gabbi et al., 2015; Painter et al., 2012; Reynolds et al., 2020; Xie et al., 2018).
27 Therefore, it is important to account for IDM when estimating the impact of dust
28 deposition on snow albedo.



1 In this study, we assess the effects of external/internal mixing of dust with ice grains on
2 the snowpack absorption coefficient and albedo using asymptotic radiative transfer
3 theory and Mie theory. In addition, the uniformity and nonuniformity of dust particle
4 distribution inside ice grains are considered for IDM, and the combined effects of dust
5 content and snow grain radius on snow albedo are quantified. A schematic of various
6 dust spatial distributions from this study is presented in Figure 2. We further discuss
7 snow albedo sensitivity to complex refractive indices and dust particle size distribution.
8 Based on a comprehensive set of field measurements of dust concentrations, we
9 estimate the reductions in snow albedo by dust external/internal mixing with ice grains
10 across the Northern Hemisphere.

11 **2 Methods**

12 **2.1 External mixing model**

13 For fairly pure snow, semi-infinite is generally defined as absorptions of about 20 cm
14 in the VIS and 3 cm in the near-infrared (NIR) regions (Zhou et al., 2003). For a semi-
15 infinite snow layer under diffuse illumination conditions, albedo can be calculated
16 using an asymptotic analysis of radiative transfer theory, which is valid in small
17 absorptions (Kokhanovsk and Zege, 2004; Zege et al., 1991):

$$18 \quad \alpha_{\lambda} = \exp(-4S_{\lambda}) \quad (1)$$

19 where α_{λ} is the spectral snow albedo, λ is the wavelength, S_{λ} is the similarity
20 parameter, and

$$21 \quad S_{\lambda} = \sqrt{\frac{\sigma_{abs}}{3\sigma_{ext}(1-g)}} \quad (2)$$

22 In Eq. (2), σ_{abs} and σ_{ext} are the absorption and extinction coefficients, respectively,
23 and g is the asymmetry parameter (the average cosine of the phase function of the
24 medium).

25 According to Eq. (18) and (25) in Kokhanovsky and Zege (2004), the extinction
26 coefficients of particles can be expressed as:

$$27 \quad \sigma_{ext} = \frac{l_{lr}}{1-g} = \frac{3C_v}{2r_{ef}} \quad (3)$$



1 where l_{tr} is the photon transport path length, $C_v = \rho_{snow}/\rho_{ice}$ is the volumetric
2 snow particle concentration, and the values $\rho_{ice} = 916.7 \text{ kg m}^{-3}$ and $\rho_{snow} = 300 \text{ kg}$
3 m^{-3} are used in subsequent calculations. r_{ef} is the effective snow grain radius, which
4 is equal to the radius of the volume-to-surface equivalent sphere ($r_{ef} = \frac{3\bar{V}}{4\bar{A}}$) where \bar{V}
5 and \bar{A} are the average volume and cross-sectional (geometric shadow) area of snow
6 grains, respectively.

7 For external dust/ice mixing (EDM) in a dust-contaminated snowpack, the total
8 absorption coefficient (σ_{abs}) can be derived from the absorptions by snow (σ_{abs}^{snow}) and
9 dust (σ_{abs}^{dust}):

$$10 \quad \sigma_{abs} = \sigma_{abs}^{snow} + \sigma_{abs}^{dust} \quad (4)$$

11 For example, consider a hypothetical case of snow composed of monodispersed,
12 spherical grains of ice. Although non-spherical snow grains lead to a slight increase in
13 snow albedo, Dang et al. (2016) found that the albedo of a snowpack consisting of non-
14 spherical snow grains can be mimicked by using smaller, spherical grains; thus, we do
15 not consider the effect of non-spherical snow grains in this study. Therefore, we used
16 the following equation for the absorption coefficient of snow (Dombrovsky and Baillis,
17 2010):

$$18 \quad \sigma_{abs}^{snow} = \frac{0.75C_v Q_{abs}^{ice}}{r_{ef}} \quad (5)$$

19 where Q_{abs}^{ice} is the efficiency factor of absorption for a single ice grain, and the value
20 of Q_{abs}^{ice} can be calculated for homogeneous spherical ice grains considered in classical
21 Mie theory.

22 The absorption coefficient of dust (Aoki et al., 2000; Marley et al., 2001; Warren et al.,
23 2006) is expressed as:

$$24 \quad \sigma_{abs}^{dust} = \frac{Q_{abs}^{dust} \cdot \pi \cdot (r_{ef}^{dust})^2}{\frac{4}{3}\pi (r_{ef}^{dust})^3} \cdot C_{dust} = \frac{3Q_{abs}^{dust}}{4r_{ef}^{dust}} \cdot C_{dust} = MAC_{abs}^{dust} \cdot \rho_{dust} \cdot C_{dust} \quad (6)$$

25 where Q_{abs}^{dust} and MAC_{abs}^{dust} is the absorption efficiency and MAC of dust,
26 respectively, that can be obtained via Mie theory, and ρ_{dust} and r_{ef}^{dust} represent the



1 density and effective dust radius, respectively. In this study, ρ_{dust} was assumed to be
2 2500 kg m^{-3} (Zender et al., 2003). We also assumed a log-normal dust size distribution
3 with a geometric mean diameter of $0.65 \mu\text{m}$ and standard deviation of 2.0 (equivalent
4 to an effective radius of $1.1 \mu\text{m}$), which represents dust from large-scale transport
5 (Formenti et al., 2011; Maring et al., 2003) that is likely smaller in size than from local
6 soil (Kok, 2011). The effects of dust size on snow optical properties and albedo were
7 further quantified through sensitivity simulations (see section 3.4). Dust volumetric
8 concentrations (C_{dust}) are expressed as:

$$9 \quad C_{dust} = \frac{\rho_{snow} \cdot C_{dust}^*}{\rho_{dust}} \quad (7)$$

10 where C_{dust}^* is the mass concentration of dust in snow (kg kg^{-1}). Thus, the spectral
11 albedo of dust-contaminated snow for EDM can be easily calculated with Eq. (1) to (7).

12 2.2 Internal mixing model

13 For the IDM (Figure 2), we first determined the effective optical constants of ice
14 containing small dust particles via an effective medium approximation (Maxwell-
15 Garnett and Larmor, 1904). According to this approach, the complex permittivity of a
16 composite medium in ice grains can be calculated in terms of particle polarizability by
17 applying the Lorentz-Lorenz formula (Koledintseva et al., 2009; Markel, 2016). We
18 used the following relationships to calculate effective complex refractive indices (RIs),
19 $m_{ef} = n_{ef} - ik_{ef}$ at known values of $m_{ice} = n_{ice} - ik_{ice}$ for pure ice and $m_{dust} = n_{dust} - ik_{dust}$
20 for dust:

$$21 \quad m_{ef}^2 = m_{ice}^2 \frac{2\delta_{dust}(m_{dust}^2 - m_{ice}^2) + m_{dust}^2 + 2m_{ice}^2}{2m_{ice}^2 + m_{dust}^2 - \delta_{dust}(m_{dust}^2 - m_{ice}^2)} \quad (8)$$

22 where δ_{dust} is the local dust fraction volume in an ice grain. We obtained the spectral
23 complex RIs of ice from Warren and Brandt (2008) and the spectral complex RIs of
24 dust from Dang et al. (2015). The imaginary part of the complex RIs of ice (k_{ice}) and
25 dust (k_{dust}) associated with absorption is shown in Figure 3. We also evaluated the effect
26 of dust on the imaginary part of the effective complex RIs (k_{ef}) assuming dust mass
27 concentrations (C_{dust}^*) of 1–100 ppm (or $\mu\text{g g}^{-1}$) in snow.



1 In all variations of the spatial distribution of dust particles in snow, the dust mass
2 concentration was assumed to be constant, which means that the local dust fraction
3 volume may differ. In an example of spherical ice grains with uniformly distributed
4 dust, the dust fraction volume in an ice grain was determined as:

$$5 \quad \delta_{dust}^0 = \frac{C_{dust}^* \rho_{ice}}{C_v \rho_{dust}} \quad (9)$$

6 where the ratio of C_{dust}^*/C_v is the mass fraction of dust in the ice grain.

7 We considered two cases of non-uniform dust distributed in a spherical ice grain with
8 radius r_{ef} : (1) We assumed that the same mass of dust is uniformly distributed in the
9 central part of the ice grain ($r_{ef}^{dust} < r_c \leq r_{ef}$). (2) We assumed all of the dust was in
10 the surface layer of the ice grain ($r_{ef}^{dust} < r_p \leq r_{ef}$) (Figure 2). In both cases the local
11 value of δ_{dust} increases as:

$$12 \quad \delta_{dust} = \delta_{dust}^0 / \psi \quad \psi = \begin{cases} \bar{r}_c^3 & \text{central pollution} \\ 1 - (1 - \bar{r}_p)^3 & \text{peripheral pollution} \end{cases} \quad (10)$$

13 where $\bar{r}_c = r_c/r_{ef}$ and $\bar{r}_p = r_p/r_{ef}$. $\bar{r}_c = 1$ and $\bar{r}_p = 1$ correspond to uniformly
14 distributed dust when $\psi = 1$ and $\delta_{dust} = \delta_{dust}^0$, and $\psi < 1$ and $\delta_{dust} > \delta_{dust}^0$ in
15 other cases. Obviously, dust particles increase the imaginary part of the effective
16 complex RIs in polluted ice grains (Figure 3).

17 In summary, the m_{ef} of a spherical ice grain with uniformly and non-uniformly
18 distributed dust can be calculated according to Eq. (8) to (10), then their corresponding
19 absorption efficiencies can be obtained using classical Mie theory and core/shell Mie
20 theory, respectively. The spectral snow albedo for IDM can be easily calculated using
21 Eq. (1) to (5).

22 2.3 Broadband snow albedo calculations

23 The spectral albedo (α_λ) is integrated over the solar spectrum ($\lambda = 300\text{--}2500$ nm) and
24 weighted by incoming solar irradiance (E_λ) to calculate broadband snow albedo (Hadley
25 and Kirchstetter, 2012):



$$1 \quad \alpha_{integrated} = \frac{\int \alpha_{\lambda} E_{\lambda} d\lambda}{\int E_{\lambda} d\lambda} \quad (11)$$

2 Following the study of Dang et al. (2017), the incoming solar irradiance we used is a
3 typical surface solar spectrum at mid to high latitudes from January to March,
4 calculated by the Santa Barbara DISORT Atmospheric Radiative Transfer (SBDART)
5 model (Pu et al., 2019). The SBDART model is a widely used atmospheric radiation
6 transfer model based on a collection of highly developed physical models, including
7 the Discrete Ordinate Radiative Transfer module (Stamnes et al., 1988), low-resolution
8 atmospheric transmission models, and Mie theory. The SBDART model can be used to
9 compute radiative transfer at different heights and directions under both clear and
10 cloudy sky conditions. Details on the SBDART model can be found in Ricchiuzzi et al.
11 (1998).

12 **2.4 Dust concentration measurements**

13 To estimate the effect of dust on snow albedo in real snowpack, we collected a
14 comprehensive set of in situ dust concentration measurements during field campaigns
15 to Inner Mongolia, China (IMC) (Wang et al., 2013), the Tibetan Plateau (TP) (Ming et
16 al., 2016; Li et al., 2017, 2018; Li et al., 2019; Niu et al., 2017; Qu et al., 2014; Zhang
17 et al., 2017, 2018), Sapporo, Japan (SJ) (Kuchiki et al., 2015), the European Alps (EP)
18 (Di Mauro et al., 2015; Lim et al., 2014), and North American mountains (NAM)
19 (Painter et al., 2012; Reynolds et al., 2020). The field campaigns conducted in the TP
20 can be further grouped into three regions, as in previous $\delta^{18}\text{O}$ precipitation studies (Yao
21 et al., 2013). These three distinct domains were associated with the Indian monsoon
22 (Southern TP), westerlies (Northern TP), and transition (Central TP) (Yao et al., 2013).
23 It is worth noting that we only considered regions with higher dust concentrations (>1
24 ppm), such that polar regions are not included in this study. Measurements of dust in
25 the snow samples were generally obtained by weighing the filter before and after
26 filtration using a microbalance.

27 **3. Results**



1 3.1 Impact on the imaginary part of the effective complex RIs

2 We evaluated the effect of dust on k_{ef} , including k_{ice} and k_{dust} associated with absorption
3 (Figure 3). The k_{dust} was in a narrow range (~ 0.001 – 0.01) and gradually decreased with
4 increasing wavelength in the ultraviolet (UV) and VIS regions, then remained stable in
5 the NIR band. The k_{ice} varied by eight orders of magnitude from the UV ($\sim 10^{-11}$) to NIR
6 ($\sim 10^{-3}$) bands, and increased with increasing wavelength, except at $1.03 \mu\text{m}$ where k_{ice}
7 decreased slightly as a result of the presence of ice absorption features (Warren, 2019).
8 Figure 3 also shows the k_{ef} with dust mass concentrations ranging from 1 to 100 ppm
9 and wavelengths of 300–1500 nm. The k_{ef} clearly varied depending on the wavelength
10 and increased with dust mass concentrations. For a given dust mass concentration, k_{ef}
11 decreased with wavelengths from UV to VIS, then increased from VIS to NIR. For
12 example, the value of k_{ef} decreased from 4.26×10^{-8} at 300 nm to 1.36×10^{-8} at 500
13 nm, then rose to 1.73×10^{-6} at 1000 nm at a dust concentration of 10 ppm. Moreover,
14 the wavelength of the valley k_{ef} value varied from ~ 500 nm to ~ 650 nm depending on
15 the dust mass concentrations (1 to 100 ppm). Additionally, it is worth noting that k_{ef} was
16 not sensitive to dust mass concentrations in wavelengths >1000 nm, which was
17 generally consistent with k_{ice} , because the order of magnitude of k_{ice} was comparable to
18 k_{dust} at those wavelengths. Conversely, k_{ef} showed significant differences relative to k_{ice}
19 in the UV and VIS regions, with higher dust mass concentrations demonstrating larger
20 differences. For example, k_{ef} was enhanced by 3, 21, and 205 times at 500 nm relative
21 to k_{ice} for dust mass concentrations of 1, 10, and 100 ppm, respectively.

22 3.2 Impact on spectral snow absorption coefficient and albedo

23 Dust in snow effectively enhances the snow absorption coefficient, but its effect on the
24 snow asymmetry factor and extinction efficiency is negligible (He et al., 2019).
25 Therefore, we mainly focused on the effects of EDM and three cases of IDM (uniform,
26 central, and peripheral) on the snow absorption coefficient (σ_{abs}). Figure 4a displays the
27 σ_{abs} for EDM and IDM (uniform) as a function of wavelength at different dust
28 concentrations. We used a snow grain radius of $200 \mu\text{m}$ (Figure 4), which is comparable



1 to previous observations of seasonal snow at mid to high latitudes in winter (Shi et al.,
2 2020; Wang et al., 2017). The results showed that EDM and IDM have distinct impacts
3 on σ_{abs} in UV and VIS, but small effects at wavelengths >1000 nm, which is due to
4 the optical properties of snow being affected by LAPs in UV and VIS and primarily
5 affected by snow itself at wavelengths >1000 nm. Additionally, σ_{abs} increased with
6 increased dust mass concentrations. For instance, σ_{abs} increased from 0.007 m^{-1} (pure
7 snow) to 0.03, 0.14, and 1.37 m^{-1} at 500 nm with 2, 10, and 100 ppm of dust with EDM,
8 respectively. For IDM (uniform), σ_{abs} increased to 0.06, 0.28, and 2.80 m^{-1} at 500 nm
9 with 2, 10, and 100 ppm of dust, respectively, with corresponding enhancement factors
10 of σ_{abs} ($E_{\sigma_{\text{abs}}}$, defined as the absorption coefficient of IDM divided by EDM) were
11 1.84, 2.00, and 2.05. Furthermore, the σ_{abs} for two cases of non-uniform dust
12 distribution in a spherical ice grain ($r_{\text{ef}} = 200 \text{ }\mu\text{m}$) can be regarded as a function of
13 wavelength, dust mass concentrations, \bar{r}_{c} , and \bar{r}_{p} (Figure 4b and 4c). We note that \bar{r}_{c}
14 and \bar{r}_{p} values of 1 correspond to uniformly distributed dust, and the σ_{abs} increases
15 and decreases (with the decrease of \bar{r}_{c} and \bar{r}_{p}) for IDM (central) and IDM (peripheral),
16 respectively. For example, σ_{abs} increased by 29%, 32%, and 33% (500 nm) at dust
17 mass concentrations of 2, 10, and 100 ppm, respectively, with \bar{r}_{c} values of 1 to 0.7 for
18 IDM (central). However, σ_{abs} decreased by 41%, 44%, and 44% (500 nm) at dust mass
19 concentrations of 2, 10, and 100 ppm, respectively, with \bar{r}_{p} of 1 to 0.1 for IDM
20 (peripheral). This indicates that the IDM (central) further enhanced snowpack light
21 absorption compared with the IDM (uniform), while the IDM (peripheral) reduced
22 snowpack light absorption with a corresponding σ_{abs} between the value of σ_{abs} for
23 IDM (uniform) and EDM. Figure 4d–f quantitatively shows the spectral snow
24 absorption coefficient enhancement for IDM ($E_{\sigma_{\text{abs}}}$). The enhancement decreased
25 sharply with increasing wavelengths, then reduced to 1.0 (i.e., no enhancement) at
26 wavelengths longer than $\sim 1.0 \text{ }\mu\text{m}$ because of strong dust absorption and weak snow
27 absorption at shorter wavelengths. Obviously, $E_{\sigma_{\text{abs}}}$ was affected by dust mass
28 concentration, \bar{r}_{c} , and \bar{r}_{p} , but $E_{\sigma_{\text{abs}}}$ was insensitive to dust mass concentration at



1 wavelengths <450 nm.

2 Figure 5a–c shows the spectral snow albedo (α_λ) for EDM and IDM; IDM was
3 consistent with σ_{abs} , with the effects mainly present at wavelengths <1000 nm.
4 Generally, α_λ decreased with increased dust mass concentrations in UV and VIS, and
5 IDM was shown to further trigger the reduction of α_λ . For example, for EDM α_λ was
6 $\sim 0.97, 0.95, 0.85$ (at 500 nm) for dust concentrations of 2, 10, 100 ppm, respectively,
7 which was higher than the values for IDM (uniform) ($\sim 0.96, 0.93, 0.79$, respectively).
8 Compared with IDM (uniform), the α_λ for IDM (central) decreased by 0.5%, 1.1%,
9 and 3.5% (at 500 nm) for dust concentrations of 2, 10, and 100 ppm, respectively, with
10 \bar{r}_c values of 1 to 0.7. α_λ for IDM (peripheral) increased by 0.8%, 1.9%, and 6.2% (at
11 500 nm) for the same dust concentrations, with \bar{r}_p from 1 to 0.1. Moreover, the
12 wavelength of the maximum α_λ value varied from ~ 500 nm to ~ 650 nm depending on
13 the dust mass concentrations, which is consistent with changes of k_{ef} . Figure 5d–f shows
14 the ratio (E_{α_λ}) of snow spectral albedo for IDM to EDM where we observed that the
15 E_{α_λ} increased with increasing wavelengths and dust concentrations, and then became
16 stable at 1.0. This is because IDM can enhance the light absorption of snowpack more
17 effectively at shorter wavelengths and higher dust concentrations (Figure 4).
18 Additionally, the values of \bar{r}_c and \bar{r}_p also have non-negligible effects on E_{α_λ} , which
19 can be decreased and increased with decreasing \bar{r}_c and \bar{r}_p , respectively.

20 We found that the optical properties of an ice grain containing uniformly distributed
21 dust in its center, or concentric surface layer, can be affected by \bar{r}_c or \bar{r}_p . To better
22 understand this effect, Figure 6a–b displays the σ_{abs} at 500 nm as a function of \bar{r}_c and
23 \bar{r}_p with different dust concentrations and r_{ef} . This demonstrates r_{ef} has negligible
24 effects on σ_{abs} due to the geometric optical limits at $r_{\text{ef}} \approx 50$ μm , which shows the
25 universal (independent of r_{ef}) monotonic dependence of σ_{abs} for ice grains with $r_{\text{ef}} \geq$
26 50 μm (Velesco et al., 1997). As a result, the spectral absorption coefficient of snow
27 containing polydispersed ice grains can be obtained using our results for a
28 monodispersed model. Interestingly, σ_{abs} did not depend on \bar{r}_c when $\bar{r}_c < 0.75$ and



1 decreased almost linearly at higher \bar{r}_c values (Figure 6a); this phenomenon can be
2 explained by geometric optical effects (Mackowski et al., 1990). However, σ_{abs} was
3 significantly affected by the dust mass concentration; for example, σ_{abs} at 500 nm was
4 decreased by 28%, 32%, and 32% from its maximum value (0.08, 0.38, and 3.71 m^{-1})
5 for concentrations of 2, 10, and 100 ppm, respectively, with $\bar{r}_c < 0.75$. The monotonic
6 increase in σ_{abs} with the relative thickness of the polluted ice grain surface layer (i.e.,
7 \bar{r}_p) was also noteworthy (Figure 6b). The core/shell Mie theory calculations for ice
8 grains with a thin surface layer ($\bar{r}_p = 0.01$) gave almost the same σ_{abs} as that obtained
9 for the EDM. As a result, the σ_{abs} increased rapidly with $\bar{r}_p < 0.4$ and then increased
10 more slowly until $\bar{r}_p = 1$, which corresponds to IDM (uniform).

11 The α_λ at 500 nm as a function of \bar{r}_c and \bar{r}_p with different dust concentrations and
12 r_{ef} , is illustrated in Figure 6c and 6d. In general, α_λ at 500 nm decreased with
13 increasing dust mass concentration and r_{ef} , the effect of grain radius can be explained
14 by increasing the forward scattering with grain size (Gardner and Sharp, 2010). For a
15 given dust mass concentration and r_{ef} , the α_λ at 500 nm increased from its minimum
16 value with $\bar{r}_c < 0.75$ to the maximum value with $\bar{r}_c = 1$, corresponding to the findings
17 of IDM (uniform). For example, at dust concentrations of 2, 10, and 100 ppm, and a
18 fixed r_{ef} of 100 μm , the α_λ at 500 nm increased by 0.2%, 0.7%, and 0.8%, respectively,
19 with \bar{r}_c from < 0.75 to 1. When the r_{ef} was fixed at 500 μm , the α_λ at 500 nm increased
20 by 1.9%, 2.5%, and 6.2% at dust concentrations of 2, 10, and 100 ppm, respectively.

21 Conversely, the α_λ at 500 nm decreased from its maximum value when $\bar{r}_p = 0.01$
22 (similar to EDM) to the minimum value with $\bar{r}_p = 1$, corresponding to the case of IDM
23 (uniform). For example, the α_λ at 500 nm decreased by 0.6%, 1.4%, and 1.4% with
24 \bar{r}_p from 0.01 to 1 for dust concentrations of 2, 10, and 100 ppm, respectively, and a
25 fixed r_{ef} of 100 μm , whereas for a r_{ef} of 500 μm , α_λ decreased by 3.3% (2 ppm dust),
26 4.7% (10 ppm), and 10.1% (100 ppm). These results indicate that dust mass
27 concentrations and r_{ef} can amplify the influence of \bar{r}_c or \bar{r}_p on snow albedo.
28 Moreover, the effect of dust mass concentration on snow albedo is similar to r_{ef} . For



1 example, dust mass concentrations of 10 and 100 ppm and r_{ef} of 100 and 50 μm gave
2 similar α_λ at 500 nm to dust mass concentrations of 2 and 10 ppm and r_{ef} of 500 μm .
3 According to this result, spectral albedo measurements at a single wavelength are
4 insufficient to obtain the mass fraction of dust in snow cover because the same effect
5 can also be explained by a combination of different ice grain sizes and a non-uniform
6 distribution of dust inside the grains. It means that additional information is needed to
7 determine accurate dust mass concentrations. This may be a set of measurements at
8 various wavelengths in the VIS and NIR spectral ranges.

9 **3.3 Effects on broadband snow albedo**

10 Compared with the spectral optical properties, broadband results can provide more
11 general knowledge for the relevant research community. Figure 7 shows the spectrally
12 weighted α_λ ($\alpha_{\text{integrated}}$) over 300–2500 nm of a typical surface solar spectrum at mid
13 to high latitudes, which is comparable with previous studies (Dang et al., 2017; Wang
14 et al., 2017). Because the results of IDM (peripheral) effects on snow albedo fell
15 between results from EDM and IDM (central), we do not consider the case of IDM
16 (peripheral) in the following discussion. Instead, we focus on the effects of dust mass
17 concentration and r_{ef} on broadband snow albedo for EDM and IDM (uniform, central).
18 Similar to α_λ , $\alpha_{\text{integrated}}$ generally decreased with increasing dust mass
19 concentrations and r_{ef} such that internal mixing declined more than external mixing.
20 $\alpha_{\text{integrated}}$ showed ranges of 0.60–0.92, 0.54–0.92, and 0.51–0.92 for EDM, IDM
21 (uniform), and IDM (central, $\bar{r}_c < 0.75$), respectively, with dust mass concentrations of
22 0–100 ppm and r_{ef} of 50–1000 μm . For a given dust mass concentration and
23 r_{ef} , $\alpha_{\text{integrated}}$ for IDM (uniform) was smaller than EDM, which is due to higher light
24 absorption in the UV and VIS bands for IDM (uniform) relative to EDM (Figure 4a).
25 While $\alpha_{\text{integrated}}$ for IDM (uniform) was larger compared with IDM (central, \bar{r}_c
26 < 0.75), this can be attributed to the fact that radiation is focused near the center of an
27 ice grain with IDM (central) (Ackerman and Toon, 1981; Bohren, 1986), enabling
28 further absorptions from inclusions near the center of a grain due to the lensing effect



1 (Mackowski et al., 1990). For example, $\alpha_{\text{integrated}}$ (dust concentration of 20 ppm, r_{ef}
2 of 500 μm) was 0.73 for IDM (uniform), less than EDM of 0.76, but higher than IDM
3 (central, $\bar{r}_c < 0.75$) of 0.72.

4 To quantify the effects of IDM on broadband snow albedo relative to EDM, we defined
5 a broadband snow albedo scaling factor ($E_{\alpha, \text{integrated}}$), which refers to the ratio of
6 $\alpha_{\text{integrated}}$ of IDM to EDM. Generally, for dust mass concentrations from 0 to 100 ppm
7 and r_{ef} of 50–1000 μm , $E_{\alpha, \text{integrated}}$ varied from 0.89 to ~ 1.00 for IDM (uniform) (Figure
8 8a) and from 0.85 to ~ 1.00 for IDM (central, $\bar{r}_c < 0.75$) (Figure 8b). $E_{\alpha, \text{integrated}}$
9 decreased significantly with increasing dust mass concentration and r_{ef} . In addition, $E_{\alpha, \text{integrated}}$
10 for IDM (central, $\bar{r}_c < 0.75$) was smaller than IDM (uniform). These results
11 have implications for the effects of IDM in real environments. For example, IMC has
12 typical dust concentrations of ~ 10 ppm (Wang et al., 2013), so $E_{\alpha, \text{integrated}}$ (r_{ef} of 50–
13 1000 μm) was 0.96–0.99 and 0.95–0.99 for IDM (uniform) and IDM (central, $\bar{r}_c <$
14 0.75), respectively. In contrast, dust concentrations are typically ~ 100 ppm in the TP
15 (Ming et al., 2016; Li et al., 2017, 2018), so $E_{\alpha, \text{integrated}}$ ranged from 0.89 to 0.98 and
16 0.85 to 0.96 for IDM (uniform) and IDM (central, $\bar{r}_c < 0.75$), respectively. The results
17 show that IDM (uniform) and IDM (central, $\bar{r}_c < 0.75$) reduced broadband snow
18 albedo by $\sim 2.5\%$ and $\sim 3.0\%$, respectively, in clean snow and $\sim 6.5\%$ and $\sim 9.5\%$,
19 respectively, in polluted snow relative to EDM. Moreover, the sensitivity of $E_{\alpha, \text{integrated}}$
20 to mineral dust decreased with increasing dust concentrations. For example, the
21 difference in $E_{\alpha, \text{integrated}}$ (r_{ef} of 500 μm) was 0.011 and 0.015 for IDM (uniform) and
22 IDM (central, $\bar{r}_c < 0.75$), respectively, when dust concentrations were 10–20 ppm, but
23 only 0.004 and 0.005 for IDM (uniform) and IDM (central, $\bar{r}_c < 0.75$), respectively,
24 when dust concentrations were 90–100 ppm. These results provide a convenient method
25 to calculate the albedo of IDM when the albedo of EDM has been obtained for a given
26 dust mass concentration and r_{ef} .

27 3.4 Uncertainties

28 Although we calculated the imaginary RI values of dust using previous studies (section



2.2), there are still large variations which strongly depend on dust composition (e.g., hematite/iron content) (Balkanski et al., 2007; Wagner et al., 2012). To roughly account for this, we estimated the influence of chosen imaginary RI values on spectrally weighted snow albedo ($E_{\alpha, \text{integrated}}$) by increasing and decreasing the calculated imaginary RI values by 50%. These changes in imaginary RIs are plausible because they are consistent with other studies (McConnell et al., 2010; Wagner et al., 2012). The results showed that $E_{\alpha, \text{integrated}}$ uncertainties attributed to the imaginary RIs of dust were $\pm 3.9\%$ and $\pm 5.2\%$ for IDM (uniform) and IDM (central, $\bar{r}_c < 0.75$), respectively. In contrast, observations have displayed large variations in the size distribution of dust in the atmosphere and snow, and this variation is strongly affected by the dust source and transport (Mahowald et al., 2014; Shao et al., 2011). In our standard simulation, we assumed a log-normal dust size distribution with a geometric mean diameter of $0.65 \mu\text{m}$ and a standard deviation of 2.0 (equivalent to an effective radius of $1.1 \mu\text{m}$), which is typical for dust transported long-range (Formenti et al., 2011; Maring et al., 2003); nearer sources of dust tend to be larger (Kok, 2011). Therefore, we investigated the effects of dust particle size on our results by assuming another two log-normal size distributions with effective radii of $2.5 \mu\text{m}$ and $5.0 \mu\text{m}$, which were within the observed size ranges in the atmosphere and snow and comparable with previously analyzed dust particle sizes (Maring et al., 2003; Shao and Mao, 2016; Zhang et al., 2003). The results showed that the uncertainty of $E_{\alpha, \text{integrated}}$ attributed to dust diameter was $\pm 6.1\%$ for both IDM (uniform) and IDM (central, $\bar{r}_c < 0.75$) because effective optical constants of ice containing small dust particles (i.e., internal mixing) are independent of dust particle size (Eq. 8). Overall, the total uncertainty of $E_{\alpha, \text{integrated}}$ from variations of imaginary RIs and dust diameter was $\pm 11.0\%$ and $\pm 11.2\%$ for IDM (uniform) and IDM (central, $\bar{r}_c < 0.75$), respectively.

3.5 Measurement-based estimate of the effects of dust on snow albedo

Finally, widespread dust concentrations in snow across the Northern Hemisphere were obtained to assess the effects of dust on snow albedo in real snowpack. Figure 9 shows



1 measured dust concentrations in snow in different regions; dust concentrations spanned
2 a broad range of values because of spatial and temporal variations in emissions,
3 transportation, and deposition among the different regions. Dust concentrations widely
4 varied from ~3 ppm to ~600 ppm, with the highest concentration in NAM and lowest
5 in the EP (Di Mauro et al., 2015; Lim et al., 2014; Painter et al., 2012; Reynolds et al.,
6 2020). However, snow samples collected in the days after a significant dust transport
7 event showed that dust concentrations in snow can be up to ~70 ppm in the EP (Di
8 Mauro et al., 2015). Additionally, the average dust concentrations in fresh snow were
9 18, 6, and 17 ppm in the southern TP, central TP, and northern TP, respectively, similar
10 to the IMC (12 ppm) (Wang et al., 2013). However, dust concentrations in aged snow
11 (120, 300, and 140 ppm) were one to two orders of magnitude higher than in fresh snow,
12 indicating the important correlation between snow type and dust concentration (Zhang
13 et al., 2017, 2018).

14 We calculated the broadband snow albedo for EDM, IDM (uniform), and IDM (central,
15 $\bar{r}_c < 0.75$) based on the measured dust concentrations (Figure 10). The results showed
16 that broadband snow albedo decreased by 0.8%, 1.4%, and 1.6% in the EP for EDM,
17 IDM (uniform), and IDM (central, $\bar{r}_c < 0.75$), respectively, which was similar to SJ.
18 However, the broadband snow albedo decreased by up to 5.6%, 8.1%, and 9.4% in the
19 EP after a significant dust transport event, indicating strong snow albedo reduction
20 during these events. In addition, broadband snow albedo was reduced by 2.0%, 3.1%,
21 and 3.6% in IMC for EDM, IDM (uniform), and IDM (central, $\bar{r}_c < 0.75$), respectively.
22 Similar results were also found for the southern TP, central TP, and northern TP where
23 the broadband snow albedo for fresh snow was reduced by 2.5%, 1.4%, and 2.5%,
24 respectively, for EDM, 3.9%, 2.1%, and 3.8% for IDM (uniform), and 4.5%, 2.4%, and
25 4.3% for IDM (central, $\bar{r}_c < 0.75$). However, the broadband snow albedo was more
26 significantly reduced for aged snow: up to 6.0%, 8.1%, and 7.5% for EDM, 9.5%,
27 11.6%, and 10.5% for IDM (uniform), and 10.9%, 13.2%, and 12.3% for IDM (central,
28 $\bar{r}_c < 0.75$) in the southern, central, and northern TP, respectively. This indicates that the



1 effects of dust on snow albedo showed stronger reductions during snowmelt periods.
2 Moreover, the largest broadband snow albedo reductions were found in NAM with
3 ranges of 9.8%–17.6%, 13.9%–24.1%, and 15.9%–27.0% for EDM, IDM (uniform),
4 and IDM (central, $\bar{r}_c < 0.75$), respectively. These results suggest that the effects of
5 external or internal dust–snow mixing on snow albedo are particularly significant for
6 the TP and NAM regions, with stronger reductions in albedo. Therefore, these results
7 can have significant impacts on both local hydrological cycles and regional climate
8 change (Oaida et al., 2015; Xie et al., 2018).

9 **4. Discussion**

10 Over the past few decades, the effects of dust in snow on reductions in albedo has been
11 widely demonstrated (Skiles et al., 2018; Zhang et al., 2018). However, the magnitude
12 of these effects has only been studied in a few regions, and uncertainties still remain.
13 Our study indicates that the albedo of dust-contaminated snowpack can be affected by
14 the dust–ice mixing state. In particular, IDM enhanced light absorption and reduced
15 snow albedo more significantly compared with EDM. For example, in IMC and the TP,
16 IDM reduced snow albedo by ~5% relative to EDM at a typical dust mass concentration
17 of 20 ppm and a snow grain radius of 500 μm . This exceeds the contribution of BC to
18 snow light absorption over most areas of North America and the Arctic (Dang et al.,
19 2017). In addition, the effects of IDM on snow albedo were amplified by higher dust
20 mass concentrations and larger snow grain sizes. We therefore strongly suggest that
21 IDM must be considered in future climate models, particularly to more accurately
22 evaluate the climate in areas where snowpack is heavily contaminated with dust and is
23 experiencing melting.

24 The mixed state between dust and snow gradually progresses from partial external
25 mixing to wholly internally mixed. Therefore, information gained solely from the
26 external mixing of dust and snow grains will underestimate the effects of dust on snow
27 albedo and radiative forcing in numerical models (e.g., Dang et al., 2015; Nagorski et
28 al., 2019). Similarly, only using information from internal mixing of dust and snow



1 grains will overestimate the effects of dust on snow albedo and radiative forcing (e.g.,
2 He et al., 2019; Liou et al., 2014). Zhao et al. (2014) underestimated the effects of dust
3 by treating wet-deposited dust as externally mixed with snow grains. In future studies,
4 we recommend the actual ratio between external and internal mixing for dust in snow
5 be examined with an environmental scanning electron microscope equipped with a cold
6 stage.

7 **5. Conclusions**

8 In this study, the effects of dust particles on absorption coefficients and snow albedo
9 were theoretically analyzed by combining asymptotic radiative transfer theory and
10 (core/shell) Mie theory. We initially considered external mixing – when dust is present
11 between ice grains – and variations of internal mixing of dust within ice grains. We
12 found that snow spectral absorption coefficients of IDM were larger than EDM across
13 UV to NIR wavelengths, but were negligible at wavelengths >1000 nm. The absorption
14 enhancement (relative to EDM) was wavelength-dependent and increased with
15 increased dust concentrations.

16 Compared with a uniform distribution of dust particles in ice grains, our calculations
17 showed that non-uniformly distributed dust particles may lead to significantly different
18 snow spectral absorption coefficients in the VIS band. Snow spectral absorption
19 coefficients were further increased when all of the dust was positioned in the central
20 part of ice grains, while the maximum absorption coefficient was found when the radius
21 of a dust-polluted core was $<75\%$ of the ice grain radius. In contrast, snow spectral
22 absorption coefficients decreased when all of the dust was positioned in the surface
23 layer of ice grains, and the minimum absorption coefficient was observed in the thin
24 surface layer of dust-polluted ice grains, which was similar for EDM. As a result,
25 broadband snow albedo decreased by up to 21%, 30%, and 33% for EDM, IDM
26 (uniform), and IDM (central, $\bar{r}_c < 0.75$), respectively, at dust concentrations of 100
27 ppm and r_{ef} of $1000 \mu\text{m}$.

28 Based on comprehensive field measurements across the Northern Hemisphere, the



1 effect of dust on snow albedo in real snowpack was evaluated by assuming external and
2 internal dust–snow mixing. The largest reductions in broadband snow albedo were in
3 NAM because that region had the highest average dust concentrations; IDM (uniform)
4 and IDM (central, $\bar{r}_c < 0.75$) further decreased snow albedo by 4.6%–7.8% and 6.8%–
5 11.4%, respectively, compared with EDM. This implies an important influence of
6 internal dust–snow mixing in NAM.

7 **Data availability**

8 The code of (core/shell) Mie theory used in this study can be found at [http://gwest.gats-](http://gwest.gats-inc.com/software/software_page.html)
9 [inc.com/software/software_page.html](http://gwest.gats-inc.com/software/software_page.html).

10 **Author contributions**

11 WX designed the study and evolved the overarching research goals and aims. STL
12 wrote the first draft with contributions from all co-authors. STL and CJC applied formal
13 techniques such as statistical, mathematical and computational to analyze study data.
14 CY collected the dust measurements across the Northern Hemisphere. ZY and PW
15 provided the majority of the methodology and software. CQL and ZXL provided
16 technical guidance. All authors contributed to the improvement of results and revised
17 the final paper.

18 **Competing interests**

19 The authors declare that they have no conflict of interest.

20 **Acknowledgments**

21 This work was supported by the National Key Research and Development Program of
22 China (grant number 2019YFA0606801) and the National Natural Science Foundation
23 of China (grant number 41975157 and 41775144).

24



1 **References**

- 2 Aoki, T., Aoki, T., Fukabori, M., Hachikubo, A., Tachibana, Y., and Nishio, F.: Effects
3 of snow physical parameters on spectral albedo and bidirectional reflectance of snow
4 surface, *J Geophys Res-Atmos*, 105, 10219-10236, 10.1029/1999jd901122, 2000.
- 5 Balkanski, Y., Schulz, M., Claquin, T., and Guibert, S.: Reevaluation of Mineral aerosol
6 radiative forcings suggests a better agreement with satellite and AERONET data, *Atmos.*
7 *Chem. Phys.*, 7, 81-95, 10.5194/acp-7-81-2007, 2007.
- 8 Casey, K. A., Kaspari, S. D., Skiles, S. M., Kreutz, K., and Handley, M. J.: The spectral
9 and chemical measurement of pollutants on snow near South Pole, Antarctica, *J*
10 *Geophys Res-Atmos*, 122, 6592-6610, 10.1002/2016jd026418, 2017.
- 11 Creamean, J. M., Suski, K. J., Rosenfeld, D., Cazorla, A., DeMott, P. J., Sullivan, R. C.,
12 White, A. B., Ralph, F. M., Minnis, P., Comstock, J. M., Tomlinson, J. M., and Prather,
13 K. A.: Dust and Biological Aerosols from the Sahara and Asia Influence Precipitation
14 in the Western U.S., *Science*, 339, 1572-1578, 10.1126/science.1227279, 2013.
- 15 Dang, C., Brandt, R. E., and Warren, S. G.: Parameterizations for narrowband and
16 broadband albedo of pure snow and snow containing mineral dust and black carbon, *J*
17 *Geophys Res-Atmos*, 120, 5446-5468, 10.1002/2014JD022646, 2015.
- 18 Dang, C., Fu, Q., and Warren, S. G.: Effect of Snow Grain Shape on Snow Albedo, *J*
19 *Atmos Sci*, 73, 3573-3583, 10.1175/JAS-D-15-0276.1, 2016.
- 20 Dang, C., Warren, S. G., Fu, Q., Doherty, S. J., Sturm, M., and Su, J.: Measurements of
21 light-absorbing particles in snow across the Arctic, North America, and China: Effects
22 on surface albedo, *J Geophys Res-Atmos*, 122, 10149-10168, 10.1002/2017jd027070,
23 2017.
- 24 DeMott, P. J., Prenni, A. J., Liu, X., Kreidenweis, S. M., Petters, M. D., Twohy, C. H.,
25 Richardson, M. S., Eidhammer, T., and Rogers, D. C.: Predicting global atmospheric
26 ice nuclei distributions and their impacts on climate, *P Natl Acad Sci USA*, 107, 11217-
27 11222, 10.1073/pnas.0910818107, 2010.
- 28 Di Mauro, B., Fava, F., Ferrero, L., Garzonio, R., Baccolo, G., Delmonte, B., and



- 1 Colombo, R.: Mineral dust impact on snow radiative properties in the European Alps
2 combining ground, UAV, and satellite observations, *J Geophys Res-Atmos*, 120, 6080-
3 6097, 10.1002/2015jd023287, 2015.
- 4 Di Mauro, B., Garzonio, R., Baccolo, G., Franzetti, A., Pittino, F., Leoni, B., Remias,
5 D., Colombo, R., and Rossini, M.: Glacier algae foster ice-albedo feedback in the
6 European Alps, *Sci Rep-Uk*, 10, 4739, 10.1038/s41598-020-61762-0, 2020.
- 7 Dombrovsky L. A., and Baillis D.: *Thermal radiation in disperse systems: an*
8 *engineering approach*. New York: Begell House, 2010.
- 9 Dombrovsky, L. A., and Kokhanovsky, A. A.: Light absorption by polluted snow cover:
10 Internal versus external mixture of soot, *Journal of Quantitative Spectroscopy and*
11 *Radiative Transfer*, 242, 106799, 10.1016/j.jqsrt.2019.106799, 2020.
- 12 Flanner, M. G., Zender, C. S., Randerson, J. T., and Rasch, P. J.: Present-day climate
13 forcing and response from black carbon in snow, *Journal of Geophysical Research*, 112,
14 10.1029/2006jd008003, 2007.
- 15 Flanner, M. G., Shell, K. M., Barlage, M., Perovich, D. K., and Tschudi, M. A.:
16 Radiative forcing and albedo feedback from the Northern Hemisphere cryosphere
17 between 1979 and 2008, *Nat Geosci*, 4, 151-155, 10.1038/ngeo1062, 2011.
- 18 Flanner, M. G., Liu, X., Zhou, C., Penner, J. E., and Jiao, C.: Enhanced solar energy
19 absorption by internally-mixed black carbon in snow grains, *Atmos Chem Phys*, 12,
20 4699-4721, 10.5194/acp-12-4699-2012, 2012.
- 21 Formenti, P., Schutz, L., Balkanski, Y., Desboeufs, K., Ebert, M., Kandler, K., Petzold,
22 A., Scheuvs, D., Weinbruch, S., and Zhang, D.: Recent progress in understanding
23 physical and chemical properties of African and Asian mineral dust, *Atmos Chem Phys*,
24 11, 8231-8256, 10.5194/acp-11-8231-2011, 2011.
- 25 France, J. L., Reay, H. J., King, M. D., Voisin, D., Jacobi, H. W., Domine, F., Beine, H.,
26 Anastasio, C., MacArthur, A., and Lee-Taylor, J.: Hydroxyl radical and NO_x production
27 rates, black carbon concentrations and light-absorbing impurities in snow from field
28 measurements of light penetration and nadir reflectivity of onshore and offshore coastal



- 1 Alaskan snow, *J Geophys Res-Atmos*, 117, 10.1029/2011jd016639, 2012.
- 2 Gabbi, J., Huss, M., Bauder, A., Cao, F., and Schwikowski, M.: The impact of Saharan
3 dust and black carbon on albedo and long-term mass balance of an Alpine glacier,
4 *Cryosphere*, 9, 1385-1400, 10.5194/tc-9-1385-2015, 2015.
- 5 Gardner, A. S., and Sharp, M. J.: A review of snow and ice albedo and the development
6 of a new physically based broadband albedo parameterization, *Journal of Geophysical*
7 *Research*, 115, 10.1029/2009jf001444, 2010.
- 8 Grenfell, T. C., Light, B., and Sturm, M.: Spatial distribution and radiative effects of
9 soot in the snow and sea ice during the SHEBA experiment, *J Geophys Res-Oceans*,
10 107, 10.1029/2000jc000414, 2002.
- 11 Hadley, O. L., and Kirchstetter, T. W.: Black-carbon reduction of snow albedo, *Nat Clim*
12 *Change*, 2, 437-440, 10.1038/nclimate1433, 2012.
- 13 Hansen, J., and Nazarenko, L.: Soot climate forcing via snow and ice albedos, *P Natl*
14 *Acad Sci USA*, 101, 423-428, 10.1073/pnas.2237157100, 2004.
- 15 He, C., Liou, K.-N., Takano, Y., Chen, F., and Barlage, M.: Enhanced Snow Absorption
16 and Albedo Reduction by Dust-Snow Internal Mixing: Modeling and Parameterization,
17 *J Adv Model Earth Sy*, n/a, 10.1029/2019ms001737, 2019.
- 18 He, C. L., Flanner, M. G., Chen, F., Barlage, M., Liou, K. N., Kang, S. C., Ming, J., and
19 Qian, Y.: Black carbon-induced snow albedo reduction over the Tibetan Plateau:
20 uncertainties from snow grain shape and aerosol-snow mixing state based on an updated
21 SNICAR model, *Atmos Chem Phys*, 18, 11507-11527, 10.5194/acp-18-11507-2018,
22 2018.
- 23 Horhold, M. W., Laepple, T., Freitag, J., Bigler, M., Fischer, H., and Kipfstuhl, S.: On
24 the impact of impurities on the densification of polar firn, *Earth Planet Sc Lett*, 325, 93-
25 99, 10.1016/j.epsl.2011.12.022, 2012.
- 26 Huang, J. P., Wang, T. H., Wang, W. C., Li, Z. Q., and Yan, H. R.: Climate effects of
27 dust aerosols over East Asian arid and semiarid regions, *J Geophys Res-Atmos*, 119,
28 11398-11416, 10.1002/2014JD021796, 2014.



- 1 Jacobson, M. Z.: Climate response of fossil fuel and biofuel soot, accounting for soot's
2 feedback to snow and sea ice albedo and emissivity, *J Geophys Res-Atmos*, 109,
3 10.1029/2004jd004945, 2004.
- 4 Kaspari, S., Skiles, S. M., Delaney, I., Dixon, D., and Painter, T. H.: Accelerated glacier
5 melt on Snow Dome, Mount Olympus, Washington, USA, due to deposition of black
6 carbon and mineral dust from wildfire, *J Geophys Res-Atmos*, 120, 2793-2807,
7 10.1002/2014jd022676, 2015.
- 8 Kok, J. F.: A scaling theory for the size distribution of emitted dust aerosols suggests
9 climate models underestimate the size of the global dust cycle, *P Natl Acad Sci USA*,
10 108, 1016-1021, 10.1073/pnas.1014798108, 2011.
- 11 Kokhanovsky, A.: Spectral reflectance of solar light from dirty snow: a simple
12 theoretical model and its validation, *Cryosphere*, 7, 1325-1331, 10.5194/tc-7-1325-
13 2013, 2013.
- 14 Kokhanovsky, A. A., and Zege, E. P.: Scattering optics of snow, *Appl Optics*, 43, 1589-
15 1602, 10.1364/AO.43.001589, 2004.
- 16 Koledintseva, M. Y., DuBroff, R. E., and Schwartz, R. W.: Maxwell Garnett Rule for
17 Dielectric Mixtures with Statistically Distributed Orientations of Inclusions, *Prog*
18 *Electromagn Res*, 99, 131-148, 10.2528/PIER09091605, 2009.
- 19 Kuchiki, K., Aoki, T., Niwano, M., Matoba, S., Kodama, Y., and Adachi, K.: Elemental
20 carbon, organic carbon, and dust concentrations in snow measured with thermal optical
21 and gravimetric methods: Variations during the 2007-2013 winters at Sapporo, Japan,
22 *J Geophys Res-Atmos*, 120, 868-882, 10.1002/2014JD022144, 2015.
- 23 Li, X. F., Kang, S. C., He, X. B., Qu, B., Tripathee, L., Jing, Z. F., Paudyal, R., Li, Y.,
24 Zhang, Y. L., Yan, F. P., Li, G., and Li, C. L.: Light-absorbing impurities accelerate
25 glacier melt in the Central Tibetan Plateau, *Sci Total Environ*, 587, 482-490,
26 10.1016/j.scitotenv.2017.02.169, 2017.
- 27 Li, X. F., Kang, S. C., Zhang, G. S., Qu, B., Tripathee, L., Paudyal, R., Jing, Z. F., Zhang,
28 Y. L., Yan, F. P., Li, G., Cui, X. Q., Xu, R., Hu, Z. F., and Li, C. L.: Light-absorbing



- 1 impurities in a southern Tibetan Plateau glacier: Variations and potential impact on
2 snow albedo and radiative forcing, *Atmos Res*, 200, 77-87,
3 10.1016/j.atmosres.2017.10.002, 2018.
- 4 Li, Y., Kang, S., Chen, J., Hu, Z., Wang, K., Paudyal, R., Liu, J., Wang, X., Qin, X., and
5 Sillanpää, M.: Black carbon in a glacier and snow cover on the northeastern Tibetan
6 Plateau: Concentrations, radiative forcing and potential source from local topsoil, *Sci*
7 *Total Environ*, 10.1016/j.scitotenv.2019.05.469, 2019.
- 8 Libois, Q., Picard, G., France, J. L., Arnaud, L., Dumont, M., Carmagnola, C. M., and
9 King, M. D.: Influence of grain shape on light penetration in snow, *Cryosphere*, 7, 1803-
10 1818, 10.5194/tc-7-1803-2013, 2013.
- 11 Lim, S., Fain, X., Zanatta, M., Cozic, J., Jaffrezo, J. L., Ginot, P., and Laj, P.: Refractory
12 black carbon mass concentrations in snow and ice: method evaluation and inter-
13 comparison with elemental carbon measurement, *Atmospheric Measurement*
14 *Techniques*, 7, 3307-3324, 10.5194/amt-7-3307-2014, 2014.
- 15 Liou, K. N., Takano, Y., and Yang, P.: Light absorption and scattering by aggregates:
16 Application to black carbon and snow grains, *J Quant Spectrosc Ra*, 112, 1581-1594,
17 10.1016/j.jqsrt.2011.03.007, 2011.
- 18 Liou, K. N., Takano, Y., He, C., Yang, P., Leung, L. R., Gu, Y., and Lee, W. L.:
19 Stochastic parameterization for light absorption by internally mixed BC/dust in snow
20 grains for application to climate models, *J Geophys Res-Atmos*, 119, 7616-7632,
21 10.1002/2014jd021665, 2014.
- 22 Mackowski, D. W., Altenkirch, R. A., and Menguc, M. P.: Internal Absorption Cross-
23 Sections in a Stratified Sphere, *Appl Optics*, 29, 1551-1559, 10.1364/AO.29.001551,
24 1990.
- 25 Mahowald, N., Albani, S., Kok, J. F., Engelstaeder, S., Scanza, R., Ward, D. S., and
26 Flanner, M. G.: The size distribution of desert dust aerosols and its impact on the Earth
27 system, *Aeolian Res*, 15, 53-71, 10.1016/j.aeolia.2013.09.002, 2014.
- 28 Maring, H., Savoie, D. L., Izaguirre, M. A., Custals, L., and Reid, J. S.: Mineral dust



- 1 aerosol size distribution change during atmospheric transport, *J Geophys Res-Atmos*,
2 108, 10.1029/2002JD002536, 2003.
- 3 Markel, V. A.: Introduction to the Maxwell Garnett approximation: tutorial, *J Opt Soc*
4 *Am A*, 33, 1244-1256, 10.1364/JOSAA.33.001244, 2016.
- 5 Marley, N. A., Gaffney, J. S., Baird, C., Blazer, C. A., Drayton, P. J., and Frederick, J.
6 E.: An empirical method for the determination of the complex refractive index of size-
7 fractionated atmospheric aerosols for radiative transfer calculations, *Aerosol Sci Tech*,
8 34, 535-549, 10.1080/02786820118599, 2001.
- 9 Matt, F. N., Burkhart, J. F., and Pietikäinen, J. P.: Modelling hydrologic impacts of light
10 absorbing aerosol deposition on snow at the catchment scale, *Hydrol. Earth Syst. Sci.*,
11 22, 179-201, 10.5194/hess-22-179-2018, 2018.
- 12 Maxwell-Garnett, J. C., and Larmor, J.: XII. Colours in metal glasses and in metallic
13 films, *Philosophical Transactions of the Royal Society of London. Series A, Containing*
14 *Papers of a Mathematical or Physical Character*, 203, 385-420, 10.1098/rsta.1904.0024,
15 1904.
- 16 McConnell, C. L., Formenti, P., Highwood, E. J., and Harrison, M. A. J.: Using aircraft
17 measurements to determine the refractive index of Saharan dust during the DODO
18 Experiments, *Atmos Chem Phys*, 10, 3081-3098, 10.5194/acp-10-3081-2010, 2010.
- 19 Ming, J., Xiao, C. D., Wang, F. T., Li, Z. Q., and Li, Y. M.: Grey Tienshan Urumqi
20 Glacier No.1 and light-absorbing impurities, *Environ Sci Pollut R*, 23, 9549-9558,
21 10.1007/s11356-016-6182-7, 2016.
- 22 Nagorski, S. A., Kaspari, S. D., Hood, E., Fellman, J. B., and Skiles, S. M. J. J. o. G. R.
23 A.: Radiative Forcing by Dust and Black Carbon on the Juneau Icefield, Alaska,
24 10.1029/2018JD029411, 2019.
- 25 Niu, H. W., Kang, S. C., Zhang, Y. L., Shi, X. Y., Shi, X. F., Wang, S. J., Li, G., Yan, X.
26 G., Pu, T., and He, Y. Q.: Distribution of light-absorbing impurities in snow of glacier
27 on Mt. Yulong, southeastern Tibetan Plateau, *Atmos Res*, 197, 474-484,
28 10.1016/j.atmosres.2017.07.004, 2017.



- 1 Niwano, M., Aoki, T., Kuchiki, K., Hosaka, M., and Kodama, Y.: Snow Metamorphism
2 and Albedo Process (SMAP) model for climate studies: Model validation using
3 meteorological and snow impurity data measured at Sapporo, Japan, *J Geophys Res-*
4 *Earth*, 117, -, 10.1029/2011jf002239, 2012.
- 5 Oaida, C. M., Xue, Y. K., Flanner, M. G., Skiles, S. M., De Sales, F., and Painter, T. H.:
6 Improving snow albedo processes in WRF/SSiB regional climate model to assess
7 impact of dust and black carbon in snow on surface energy balance and hydrology over
8 western US, *J Geophys Res-Atmos*, 120, 3228-3248, 10.1002/2014JD022444, 2015.
- 9 Painter, T. H., Skiles, S. M., Deems, J. S., Bryant, A. C., and Landry, C. C.: Dust
10 radiative forcing in snow of the Upper Colorado River Basin: 1. A 6 year record of
11 energy balance, radiation, and dust concentrations, *Water Resour Res*, 48,
12 10.1029/2012WR011985, 2012.
- 13 Pu, W., Cui, J., Shi, T., Zhang, X., He, C., and Wang, X.: The remote sensing of radiative
14 forcing by light-absorbing particles (LAPs) in seasonal snow over northeastern China,
15 *Atmos. Chem. Phys.*, 19, 9949-9968, 10.5194/acp-19-9949-2019, 2019.
- 16 Qian, Y., Yasunari, T. J., Doherty, S. J., Flanner, M. G., Lau, W. K. M., Ming, J., Wang,
17 H. L., Wang, M., Warren, S. G., and Zhang, R. D.: Light-absorbing Particles in Snow
18 and Ice: Measurement and Modeling of Climatic and Hydrological impact, *Advances*
19 *in Atmospheric Sciences*, 32, 64-91, 10.1007/s00376-014-0010-0, 2015.
- 20 Qu, B., Ming, J., Kang, S. C., Zhang, G. S., Li, Y. W., Li, C. D., Zhao, S. Y., Ji, Z. M.,
21 and Cao, J. J.: The decreasing albedo of the Zhadang glacier on western
22 Nyainqentanglha and the role of light-absorbing impurities, *Atmos Chem Phys*, 14,
23 11117-11128, 10.5194/acp-14-11117-2014, 2014.
- 24 Rahimi, S., Liu, X., Wu, C., Lau, W. K., Brown, H., Wu, M., and Qian, Y.: Quantifying
25 snow darkening and atmospheric radiative effects of black carbon and dust on the South
26 Asian monsoon and hydrological cycle: experiments using variable-resolution CESM,
27 *Atmos. Chem. Phys.*, 19, 12025-12049, 10.5194/acp-19-12025-2019, 2019.
- 28 Rango, A., Wergin, W. P., and Erbe, E. F.: Snow crystal imaging using scanning electron



- 1 microscopy .2. Metamorphosed snow, *Hydrolog Sci J*, 41, 235-250,
2 10.1080/02626669609491495, 1996.
- 3 Reay, H. J., France, J. L., and King, M. D.: Decreased albedo, e-folding depth and
4 photolytic OH radical and NO₂ production with increasing black carbon content in
5 Arctic snow, *J Geophys Res-Atmos*, 117, 10.1029/2011jd016630, 2012.
- 6 Reynolds, R. L., Goldstein, H. L., Moskowitz, B. M., Kokaly, R. F., Munson, S. M.,
7 Solheid, P., Breit, G. N., Lawrence, C. R., and Derry, J.: Dust deposited on snow cover
8 in the San Juan Mountains, Colorado, 2011-2016: Compositional variability bearing on
9 snow-melt effects, *Journal of Geophysical Research: Atmospheres*, n/a,
10 e2019JD032210, 10.1029/2019JD032210, 2020.
- 11 Ricchiazzi, P., Yang, S. R., Gautier, C., and Sowle, D.: SBDART: A research and
12 teaching software tool for plane-parallel radiative transfer in the Earth's atmosphere,
13 *Bulletin of the American Meteorological Society*, 79, 2101-2114, 10.1175/1520-
14 0477(1998)079<2101:Sarats>2.0.Co;2, 1998.
- 15 Shao, J. F., and Mao, J. D.: Dust Particle Size Distributions during Spring in Yinchuan,
16 China, *Adv Meteorol*, 2016, 10.1155/2016/6940502, 2016.
- 17 Shao, Y. P., Wyrwoll, K. H., Chappell, A., Huang, J. P., Lin, Z. H., McTainsh, G. H.,
18 Mikami, M., Tanaka, T. Y., Wang, X. L., and Yoon, S.: Dust cycle: An emerging core
19 theme in Earth system science, *Aeolian Res*, 2, 181-204, 10.1016/j.aeolia.2011.02.001,
20 2011.
- 21 Shi, T., Pu, W., Zhou, Y., Cui, J., Zhang, D., and Wang, X.: Albedo of Black Carbon-
22 Contaminated Snow Across Northwestern China and the Validation With Model
23 Simulation, *Journal of Geophysical Research: Atmospheres*, 125, e2019JD032065,
24 10.1029/2019JD032065, 2020.
- 25 Skiles, S. M., Flanner, M., Cook, J. M., Dumont, M., and Painter, T. H.: Radiative
26 forcing by light-absorbing particles in snow, *Nat Clim Change*, 1, 10.1038/s41558-018-
27 0296-5, 2018.
- 28 Spaulding, N. E., Meese, D. A., and Baker, I.: Advanced microstructural



- 1 characterization of four East Antarctic firn/ice cores, *J Glaciol*, 57, 796-810,
2 10.3189/002214311798043807, 2011.
- 3 Stamnes, K., Tsay, S. C., Wiscombe, W., and Jayaweera, K.: Numerically Stable
4 Algorithm for Discrete-Ordinate-Method Radiative-Transfer in Multiple-Scattering
5 and Emitting Layered Media, *Appl Optics*, 27, 2502-2509, 10.1364/Ao.27.002502,
6 1988.
- 7 Usha, K. H., Nair, V. S., and Babu, S. S.: Modeling of aerosol induced snow albedo
8 feedbacks over the Himalayas and its implications on regional climate, *Climate
9 Dynamics*, 10.1007/s00382-020-05222-5, 2020.
- 10 Velesco, N., Kaiser, T., and Schweiger, G.: Computation of the internal field of a large
11 spherical particle by use of the geometrical-optics approximation, *Appl Optics*, 36,
12 8724-8728, 10.1364/AO.36.008724, 1997.
- 13 Wagner, R., Ajtai, T., Kandler, K., Lieke, K., Linke, C., Müller, T., Schnaiter, M., and
14 Vragel, M.: Complex refractive indices of Saharan dust samples at visible and near UV
15 wavelengths: a laboratory study, *Atmos. Chem. Phys.*, 12, 2491-2512, 10.5194/acp-12-
16 2491-2012, 2012.
- 17 Wang, X., Doherty, S. J., and Huang, J.: Black carbon and other light-absorbing
18 impurities in snow across Northern China, *Journal of Geophysical Research:
19 Atmospheres*, 118, 1471-1492, 10.1029/2012jd018291, 2013.
- 20 Wang, X., Pu, W., Ren, Y., Zhang, X., Zhang, X., Shi, J., Jin, H., Dai, M., and Chen, Q.:
21 Observations and model simulations of snow albedo reduction in seasonal snow due to
22 insoluble light-absorbing particles during 2014 Chinese survey, *Atmos Chem Phys*, 17,
23 2279-2296, 10.5194/acp-17-2279-2017, 2017.
- 24 Warren, S. G., and Wiscombe, W. J.: A Model for the Spectral Albedo of Snow .2. Snow
25 Containing Atmospheric Aerosols, *J Atmos Sci*, 37, 2734-2745, 10.1175/1520-
26 0469(1980)037<2734:Amftsa>2.0.Co;2, 1980.
- 27 Warren, S. G.: Impurities in Snow - Effects on Albedo and Snowmelt Review, *Ann
28 Glaciol*, 5, 177-179, 10.3189/1984AoG5-1-177-179, 1984.



- 1 Warren, S. G., Brandt, R. E., and Grenfell, T. C.: Visible and near-ultraviolet absorption
2 spectrum of ice from transmission of solar radiation into snow, *Appl Optics*, 45, 5320-
3 5334, 10.1364/Ao.45.005320, 2006.
- 4 Warren, S. G., and Brandt, R. E.: Optical constants of ice from the ultraviolet to the
5 microwave: A revised compilation, *J Geophys Res-Atmos*, 113,
6 10.1029/2007JD009744, 2008.
- 7 Warren, S. G.: Optical properties of ice and snow, *Philos T R Soc A*, 377,
8 10.1098/rsta.2018.0161, 2019.
- 9 Xie, X. N., Liu, X. D., Che, H. Z., Xie, X. X., Li, X. Z., Shi, Z. G., Wang, H. L., Zhao,
10 T. L., and Liu, Y. G.: Radiative feedbacks of dust in snow over eastern Asia in CAM4-
11 BAM, *Atmos Chem Phys*, 18, 12683-12698, 10.5194/acp-18-12683-2018, 2018.
- 12 Yao, T. D., Masson-Delmotte, V., Gao, J., Yu, W. S., Yang, X. X., Risi, C., Sturm, C.,
13 Werner, M., Zhao, H. B., He, Y., Ren, W., Tian, L. D., Shi, C. M., and Hou, S. G.: A
14 review of climatic controls on $\delta^{18}\text{O}$ in precipitation over the Tibetan Plateau:
15 Observations and simulations, *Reviews of Geophysics*, 51, 10.1002/rog.20023, 2013.
- 16 Yasunari, T. J., Koster, R. D., Lau, K. M., Aoki, T., Sud, Y. C., Yamazaki, T., Motoyoshi,
17 H., and Kodama, Y.: Influence of dust and black carbon on the snow albedo in the
18 NASA Goddard Earth Observing System version 5 land surface model, *J Geophys Res-*
19 *Atmos*, 117, 10.1029/2012jd018691, 2012.
- 20 Yasunari, T. J., Koster, R. D., Lau, W. K. M., and Kim, K. M.: Impact of snow darkening
21 via dust, black carbon, and organic carbon on boreal spring climate in the Earth system,
22 *J Geophys Res-Atmos*, 120, 5485-5503, 10.1002/2014jd022977, 2015.
- 23 Zege, E. P., Ivanov, A. P., and Katsev, I. L.: *Image transfer through a scattering medium*.
24 Berlin, Springer-Verlag, 1991.
- 25 Zender, C. S., Bian, H. S., and Newman, D.: Mineral Dust Entrainment and Deposition
26 (DEAD) model: Description and 1990s dust climatology, *J Geophys Res-Atmos*, 108,
27 10.1029/2002JD002775, 2003.
- 28 Zhang, D., Iwasaka, Y., Shi, G., Zang, J., Matsuki, A., and Trochkin, D.: Mixture state



1 and size of Asian dust particles collected at southwestern Japan in spring 2000, Journal
2 of Geophysical Research: Atmospheres, 108, 10.1029/2003JD003869, 2003.

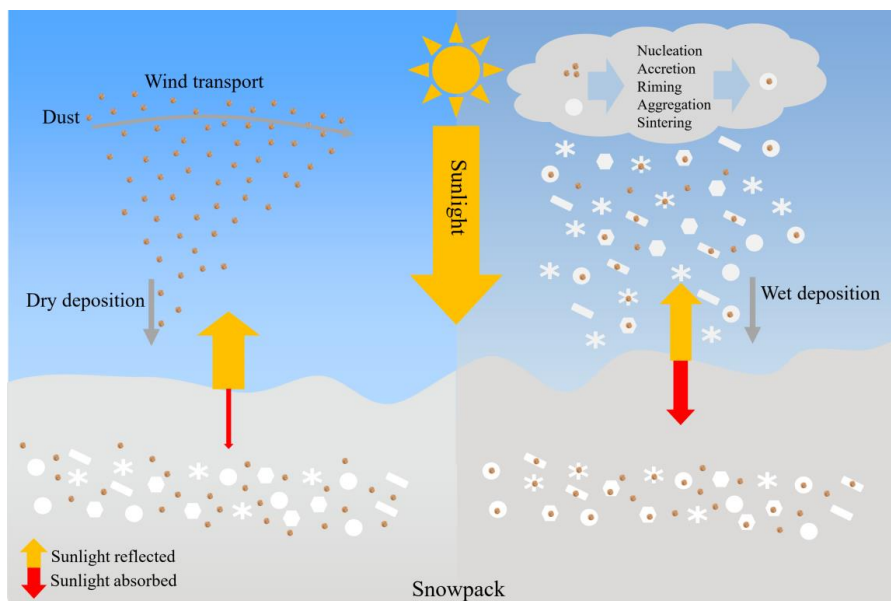
3 Zhang, Y. L., Kang, S. C., Cong, Z. Y., Schmale, J., Sprenger, M., Li, C. L., Yang, W.,
4 Gao, T. G., Sillanpaa, M., Li, X. F., Liu, Y. J., Chen, P. F., and Zhang, X. L.: Light-
5 absorbing impurities enhance glacier albedo reduction in the southeastern Tibetan
6 plateau, J Geophys Res-Atmos, 122, 6915-6933, 10.1002/2016jd026397, 2017.

7 Zhang, Y. L., Kang, S. C., Sprenger, M., Cong, Z. Y., Gao, T. G., Li, C. L., Tao, S., Li,
8 X. F., Zhong, X. Y., Xu, M., Meng, W. J., Neupane, B., Qin, X., and Sillanpaa, M.:
9 Black carbon and mineral dust in snow cover on the Tibetan Plateau, Cryosphere, 12,
10 413-431, 10.5194/tc-12-413-2018, 2018.

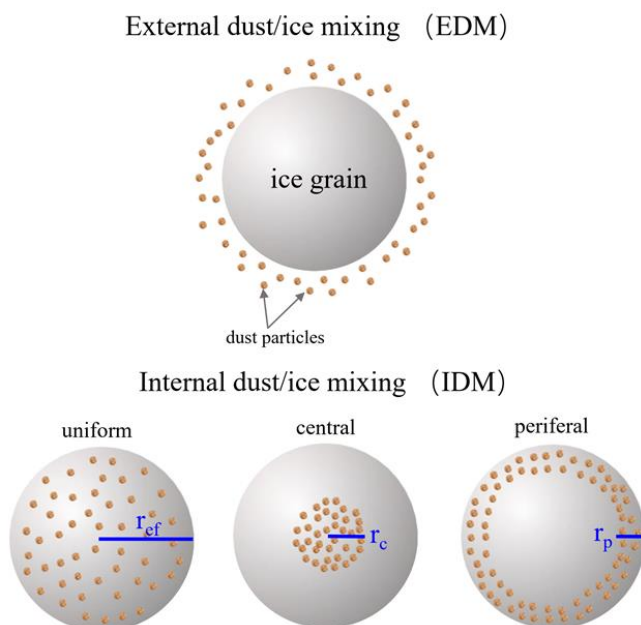
11 Zhao, C., Hu, Z., Qian, Y., Leung, L. R., Huang, J., Huang, M., Jin, J., Flanner, M. G.,
12 Zhang, R., Wang, H., Yan, H., Lu, Z., and Streets, D. G.: Simulating black carbon and
13 dust and their radiative forcing in seasonal snow: a case study over North China with
14 field campaign measurements, Atmos Chem Phys, 14, 11475-11491, 10.5194/acp-14-
15 11475-2014, 2014.

16 Zhou, X. B., Li, S. S., and Stamnes, K.: Effects of vertical inhomogeneity on snow
17 spectral albedo and its implication for optical remote sensing of snow, J Geophys Res-
18 Atmos, 108, 10.1029/2003JD003859, 2003.

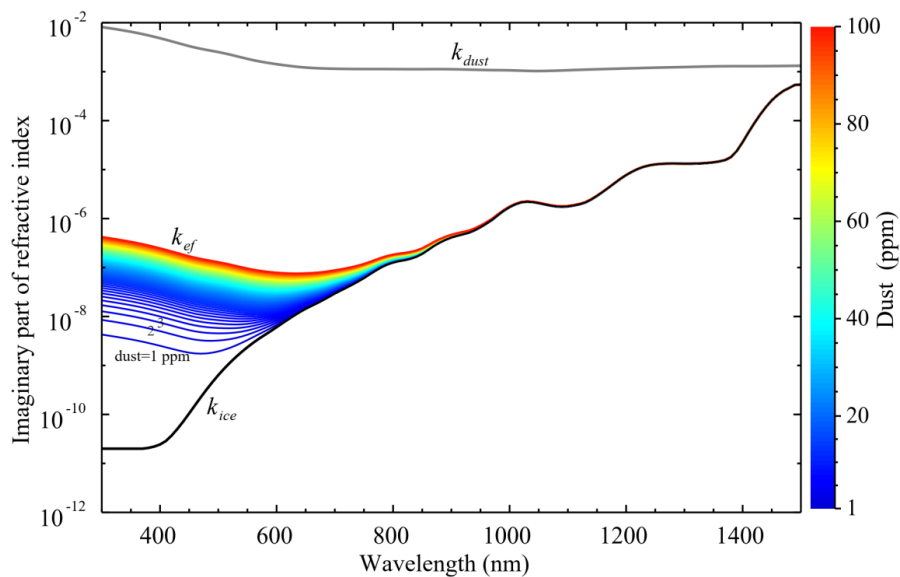
19



1
2 **Figure 1.** Schematic of dust mixing with snow grains internally. Dust tends to mix
3 externally with snow grains through dry deposition and/or below cloud scavenging,
4 while dust–snow internal mixtures can be produced by nucleation, accretion, riming,
5 aggregation, and sintering during aerosol–cloud–precipitation processes known as wet
6 deposition. Arrows represent how the absorption (red) and reflection (yellow) of
7 incoming sunlight changes with dust–snow mixing state.
8



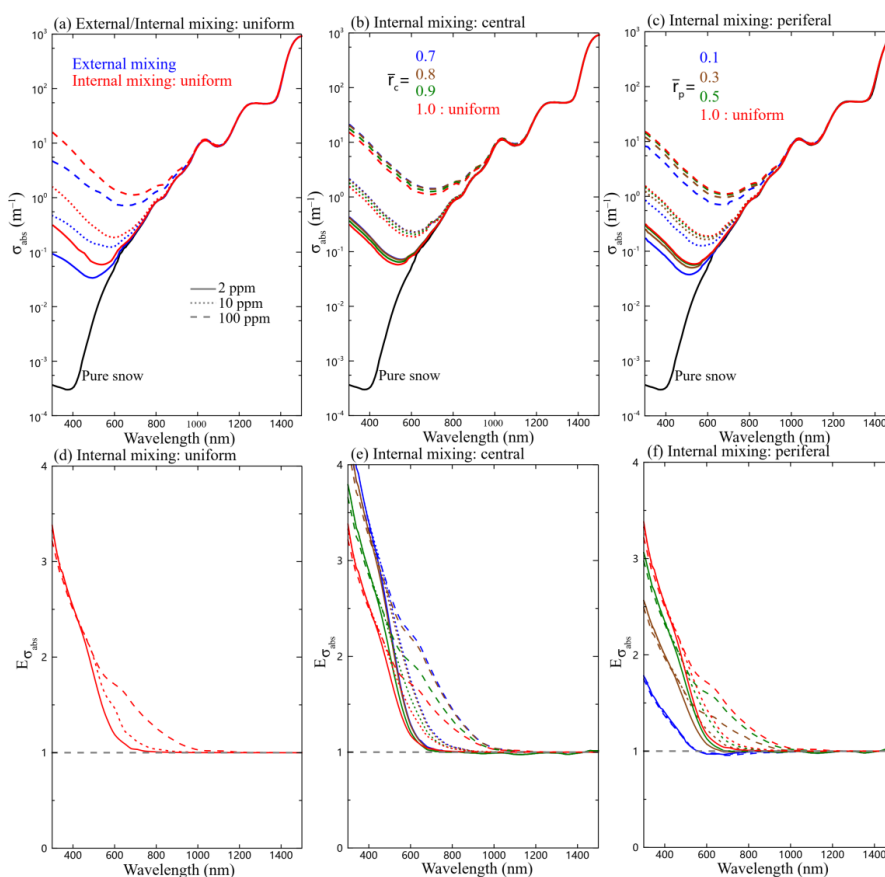
1
2 **Figure 2.** Schematic depicting various mixing scenarios of snow grains and dust
3 particles.
4



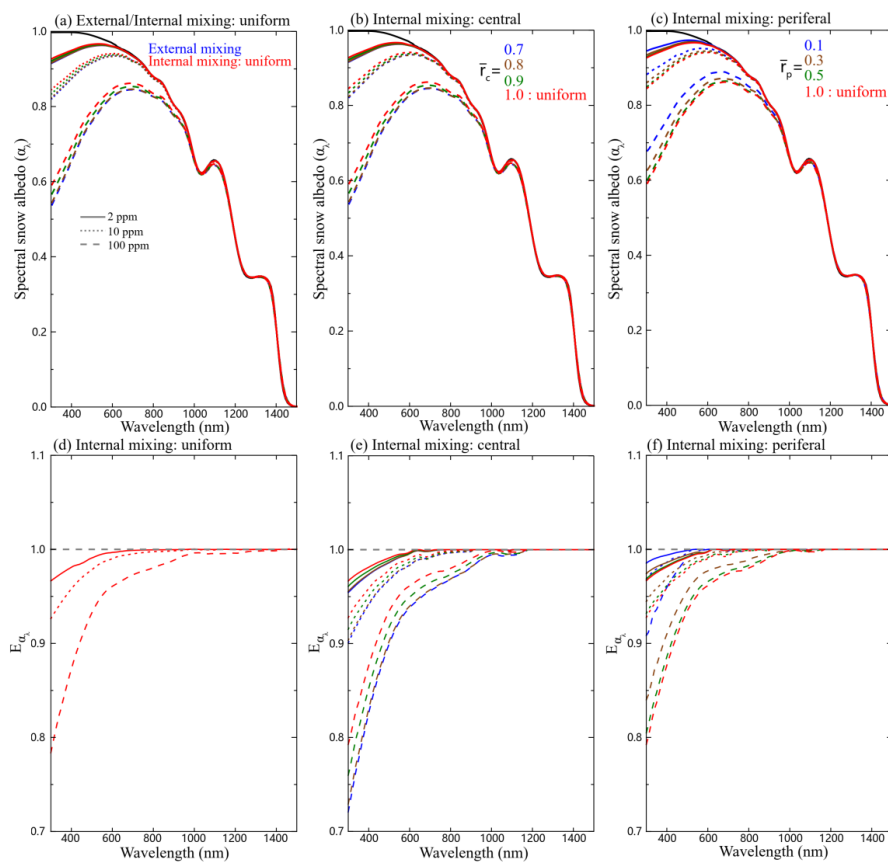
1

2 **Figure 3.** Imaginary part of the spectral complex refractive indices of ice (k_{ice}) and dust
3 (k_{dust}) (Warren and Brandt, 2008; Dang et al., 2015), with the imaginary part of the
4 effective complex refractive indices (k_{ef}) as a function of wavelength, at dust mass
5 concentrations (C_{dust}^*) of 1–100 ppm (or $\mu\text{g g}^{-1}$) in snow.

6



1
 2 **Figure 4.** Snow absorption coefficients (σ_{abs}) for dust–snow (a) external and internal
 3 mixing (uniform), (b) internal mixing (central), and (c) internal mixing (peripheral), as
 4 a function of wavelength with different dust concentrations and \bar{r}_c and \bar{r}_p . The
 5 corresponding enhancement ($E_{\sigma_{\text{abs}}}$) caused by (d) internal mixing (uniform), (e) internal
 6 mixing (central), and (f) internal mixing (peripheral) relative to external mixing, is
 7 shown as a function of wavelength. The snow grain radius was assumed to be 200 μm .
 8

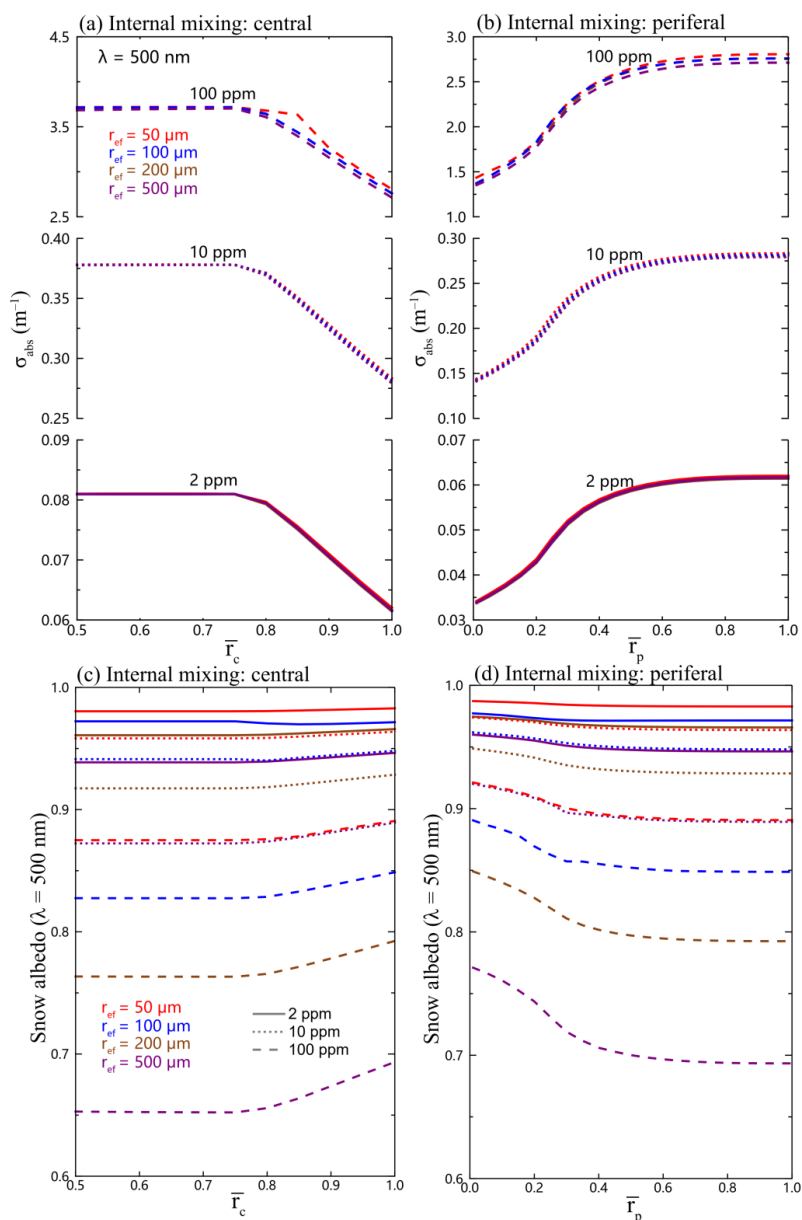


1

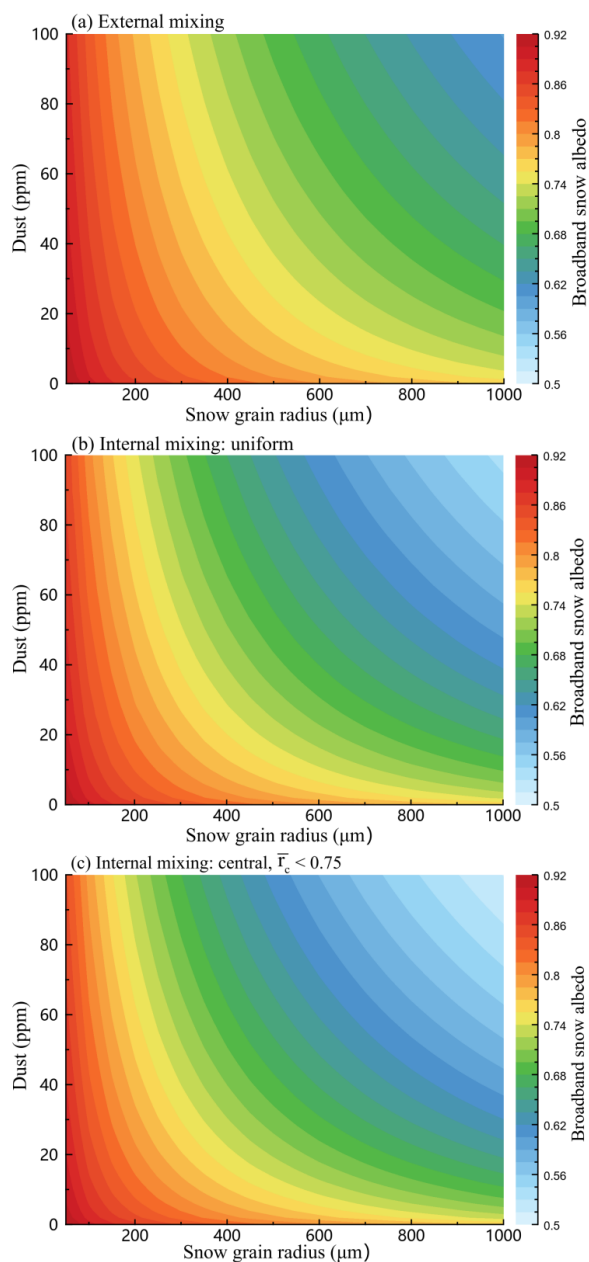
2

Figure 5. Same as Figure 4, but for spectral snow albedo (α_λ).

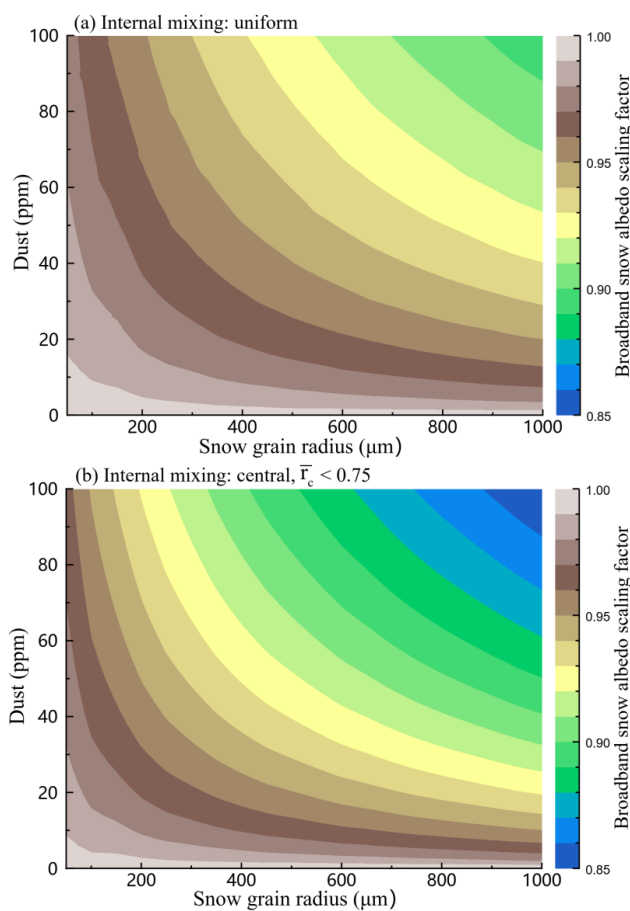
3



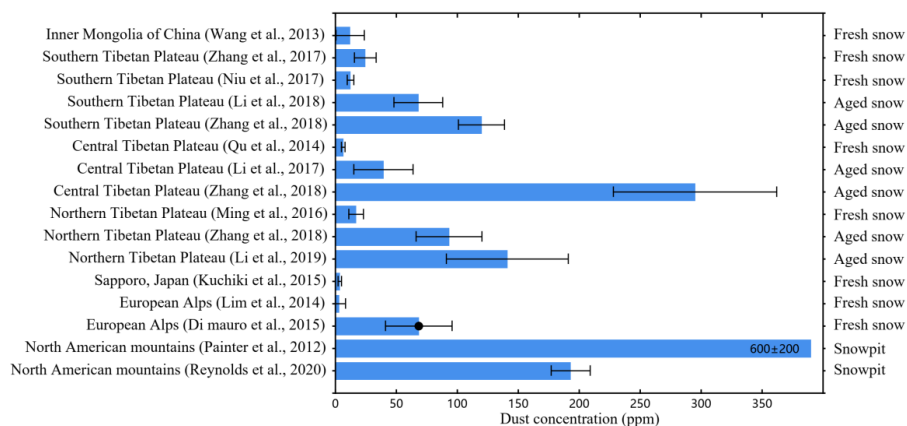
1
 2 **Figure 6.** The snow absorption coefficient (σ_{abs}) at 500 nm wavelength as a function of
 3 $\bar{\Gamma}_c$ and $\bar{\Gamma}_p$ for (a) internal mixing (central) and (b) internal mixing (peripheral) with
 4 different snow grain radii and dust mass concentrations. (d) and (e) are the same as (a)
 5 and (b), but for snow albedo at 500 nm wavelength.
 6



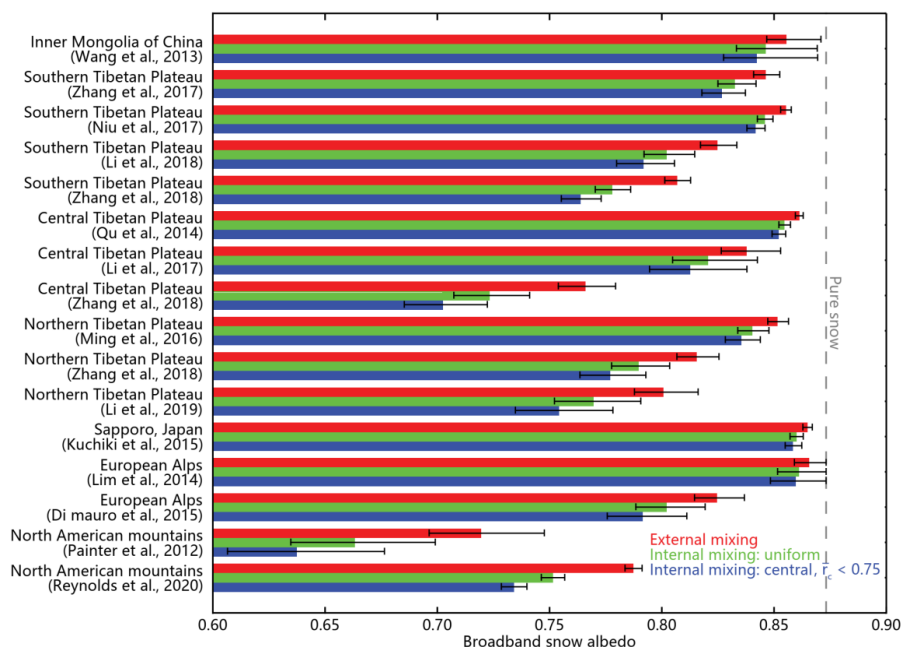
1
2 **Figure 7.** Broadband snow albedo ($\alpha_{\text{integrated}}$) variations affected by different dust
3 mass concentrations and snow grain radii for (a) external mixing, (b) internal mixing
4 (uniform), and (c) internal mixing (central, $\bar{r}_c < 0.75$).
5



1
2 **Figure 8.** Variations in the broadband snow albedo scaling factor ($E_{\alpha, \text{integrated}}$, ratio of
3 $\alpha_{\text{integrated}}$ for IDM to EDM) due to different dust mass concentrations and snow grain
4 radii for (a) internal mixing (uniform) and (b) internal mixing (central, $\bar{r}_c < 0.75$).
5



1
2 **Figure 9.** In situ measurements of dust concentrations in snow (fresh snow, aged snow,
3 and snowpit from field sampling in different regions of the Northern Hemisphere. The
4 solid black circle represents snow samples that were collected days after a significant
5 dust transport event.
6



1
2
3
4
5
6

Figure 10. Calculated broadband snow albedo based on dust concentration measurements in different areas for dust–snow external mixing, internal mixing (uniform), and internal mixing (central, $\bar{r}_c < 0.75$). The dashed line represents broadband albedo of pure snow, and the snow grain radius was assumed to be 200 μm .